Environment International 134 (2020) 105301

Contents lists available at ScienceDirect

Environment International

journal homepage: www.elsevier.com/locate/envint

Application of satellite remote sensing in monitoring dissolved oxygen variabilities: A case study for coastal waters in Korea

Yong Hoon Kim[a], Seunghyun Son[b], Hae-Cheol Kim[c], Bora Kim[d], Young-Gyu Park[e], Jungho Nam[f], Jongseong Ryu[d,*]

[a] Department of Earth and Space Sciences, West Chester University of Pennsylvania, West Chester, PA, USA
[b] CIRA at NOAA/NESDIS/STAR, Fort Collins, CO, USA
[c] UCAR at NOAA/GFDL, Princeton, NJ, USA
[d] Department of Marine Biotechnology, Anyang University, Ganghwa-gun, Incheon, Republic of Korea
[e] Korea Institute of Ocean Science and Technology, Busan, Republic of Korea
[f] Korea Maritime Institute, Busan, Republic of Korea

ARTICLE INFO

Handling Editor: Adrian Covaci

Keywords:
Remote sensing
Satellite
Dissolved oxygen
Multiple regression
Yellow Sea

ABSTRACT

Dissolved oxygen (DO) is one of the critical parameters representing water quality in coastal environments. However, it is labor- and cost-intensive to maintain monitoring systems of DO since *in situ* measurements of DO are needed in high spatial and temporal resolution to establish proper management plans of coastal regions. In this study, we applied statistical analyses between long-term monitoring datasets and satellite remote sensing datasets in the eastern coastal region of the Yellow Sea. Pearson correlation analysis of long-term water quality monitoring datasets shows that water temperature and DO are highly correlated. Stepwise multiple regression analysis among DO and satellite-derived environmental variables shows that the *in situ* DO can be estimated by the combination of the present sea surface temperature (SST), the chlorophyll-*a*, and the SST in the month prior. The high skill score of our proposed model to derive DO is validated by two error measures, the Absolute Relative Error, 1-ARE (89.2%), and Index of Agreement, IOA (78.6%). By applying the developed model to the Moderate Resolution Imaging Spectroradiometer (MODIS) and Visible Infrared Imaging Radiometer Suite (VIIRS) products, spatial and temporal changes in satellite-derived DO can be observed in Saemangeum offshore in the Yellow Sea. The analysis results show that there is a significant decrease in estimated DO between summer of 2003 versus 2012 indicating summer coastal deoxygenation due probably to the Saemangeum reclamation. This study shows the potential capability of satellite remote sensing in monitoring *in situ* DO in both high temporal and spatial resolution, which will be beneficial for effective and efficient management of coastal environments.

1. Introduction

Dissolved oxygen (DO) in coastal waters has been declining in past centuries, caused largely by the increases of both ocean temperature and nutrients inputs attributed to human activities (Breitburg et al., 2018; Diaz and Rosenberg, 2008). Declines of DO have been the subject of recent discussion because they have negative impacts on marine ecosystems (Rabalais et al., 2001) and biogeochemical processes (Rabalais, 2004; Middelburg and Levin, 2009), which subsequently change ocean productivity and biodiversity, for example, salmonid embryos (Doudoroff and Shumway, 1970). Deoxygenation in the open ocean has only been recently reported (Keeling et al., 2010), while extensive DO changes in coastal areas have been known for a long time (Diaz and Rosenberg, 2008). These changes can be considered critical stressors in coastal and oceanic environments, coupled with other environmental stressors such as ocean warming and acidification (Farrel, 2016; Gobler and Baumann, 2016). Proper management to protect ecosystem services requires extensive observations, effective analysis, and improved prediction of DO in both coastal and ocean systems.

Observing and monitoring changes in spatio-temporal patterns of DO in coastal systems have become crucial to evaluating the water quality in coastal environments (Breitburg et al., 2018). However, this is inherently difficult to measure DO with high spatial and temporal resolution. Recently, satellite remote sensing techniques are more frequently applied to collect water quality information (Goetz et al., 2008; Choi et al., 2012; Kim et al., 2014; Kim et al., 2017). The advantages of

* Corresponding authors.
E-mail addresses: jhnam@kmi.re.kr (J. Nam), jsryu@anyang.ac.kr (J. Ryu).

https://doi.org/10.1016/j.envint.2019.105301
Received 30 July 2019; Received in revised form 14 October 2019; Accepted 30 October 2019
Available online 16 November 2019

remotely sensed datasets over *in situ* measured ones are an increased temporal frequency and a greater spatial coverage, providing synoptic and consistent data sets useful for integrated analysis, which is critical for environmental management and planning.

The environmental variables that can be estimated by satellite remote sensed data have been limited to their optical properties based on visible (e.g., suspended sediments, colored dissolved organic matters; Kim et al., 2014; Miller and McKee, 2004; Siswanto et al., 2011; Zhang et al., 2010), near-infrared (e.g., chlorophyll-a; Harvey et al., 2015; Hellweger et al., 2004; Shen et al., 2012; Son and Wang, 2012), and infrared (e.g., sea surface temperature; Kilpatrick et al., 2015; Kim et al., 2017; Minnett et al., 2004) signals. Since the relationship between other water quality data (e.g., nutrients, chemical oxygen demands, and DO) and satellite data is too complex to be modeled (Gholizadeh et al., 2016), artificial intelligence frameworks, including neural networks and machine learning, have been applied to estimate recent water quality measurements (e.g., Kim et al., 2014; Sharaf El Din et al., 2017). None of these studies, however, attempted to apply a linear relationship between satellite data and specific water quality variables.

This study attempts to extend the application of satellite remote sensing techniques to retrieve DO concentration in coastal surface waters by using a multiple-regression approach. Multiple level-2 products of ocean color sensors, such as Moderate Resolution Imaging Spectroradiometer (MODIS) and the Visible Infrared Imaging Radiometer Suite (VIIRS), are correlated with long-term environmental monitoring datasets in the eastern coastal region of the Yellow Sea. The multiple regression model developed here is applied to produce high temporal-and spatial-resolution satellite-derived DO data. For the case study, the satellite-derived DO data are used to show the change in coastal water quality before and after one of the world's largest reclamation projects (Saemangeum). The next two sections describe the study area and the methodology used for this study. Analysis and findings are presented and discussed in the Results and Discussion. The last section summarizes conclusions.

2. Materials and methods

2.1. Study area

The west coast of Korea (eastern Yellow Sea) is characterized by the macrotidal condition up to ~10 m tidal height at spring tide (Choi and Kim, 2006; Hwang et al., 2014). The current study targeted the macrotidal regime area (tidal range = 1.2–7.2 m) near the mouth of the Geum River estuary (A in Fig. 1), nearshore of Saemangeum dike (B and C in Fig. 1), and offshore (D in Fig. 1). These areas were selected to represent various conditions of coastal environments, including estuarine, nearshore, and offshore conditions.

Until the construction of the dike, the study area was originally characterized by huge estuarine and tidal flat regions (~400 km^2) off the mouths of two rivers, the Mangyeong and Dongjin Rivers. The area has undergone extensive reclamation, including the world's longest sea dike (33.9 km) completed in 2006. A significant amount of freshwater still flows into the lake, subsequently flowing into the Yellow Sea via the two sluice gates (Lee et al., 2008). Before dike construction, large tidal flats covered an area of ~233 km^2 inside the dike, with a width of 5 km in many places, extending to a maximum of 15 km at the mouth of the estuary (Ryu et al., 2011).

2.2. In-situ field monitoring dataset

The *in situ* measured water quality data in surface waters off of the dike and near the Geum River mouth were collected as part of the Marine Environmental Monitoring System of Korea (K-MEMS) from August 2002 to December 2016 (http://www.meis.go.kr). According to the Korean water quality manual, A total of 15 stations were seasonally

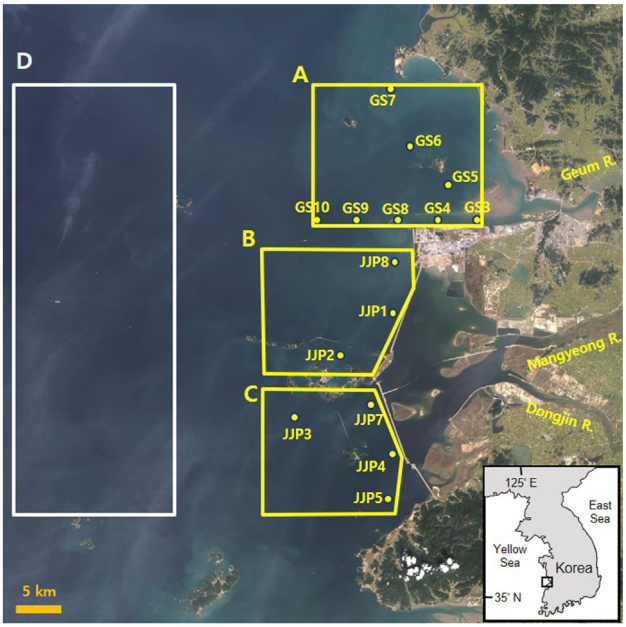

Fig. 1. Study area including K-MEMS monitoring stations (represented by dots) and boxes for the satellite data extraction for model development (yellow) and application (white). (For interpretation of the references to colour in this figure legend, the reader is referred to the web version of this article.)

monitored by field instruments, which measured water temperature, salinity, pH, DO, and Secchi depth, and by laboratory experiments providing suspended sediments (SS), chlorophyll-a (Chl-a), chemical oxygen demands (COD), ammonia, nitrite, nitrate, dissolved inorganic nitrogen (DIN), total nitrogen (TN), dissolved inorganic phosphorus (DIP), total phosphorus (TP), and silicate (Ministry of Oceans and Fisheries, 2013a). The *in situ* observation occurred every three months, in February, May, August and November, representing each season.

In situ monitoring stations are divided into three groups (Fig. 1); region A (eight stations) representing the region under the influence of the Geum River, regions B (three stations) representing nearshore of the northern dike, and region C (four stations) representing nearshore of the southern dike where two watergates were located. A total of 806 observation data were collected from 15 stations and used for time-series presentation in 2002–2016. Data collected from the stations in each region were spatially averaged for each sampling month, which were then used for correlation and multiple regression analyses (model development). Region D representing offshore was used for model application only since *in situ* monitoring station does not exist. To compare averages of 16 *in situ* water quality parameters before and after the dike construction in 2006, one-way ANOVA and post-hoc test were conducted using SPSS 12.0. In case of equal variances among datasets, ANOVA and least significant difference (LSD) test were conducted. In case of unequal variances, Welch's test and Games-Howell nonparametric test were applied. (Table S1).

2.3. Satellite remote sensing dataset

The NASA Ocean Biology Processing Group (OBPG) provides the MODIS onboard the Aqua and the VIIRS onboard the Suomi National Polar-orbit Partnership (SNPP) through the NASA ocean color website (http://oceancolor.gsfc.nasa.gov/). Daily Level-2 Chl-a concentration and remote sensing reflectance (R_{rs}) at various wavelengths ($R_{rs}(\lambda)$), and daytime sea surface temperature (SST) from the MODIS-Aqua and the VIIRS sensors passing over the Korean west coasts including the Saemangeum area and the Geum River were obtained for the periods of July 2002 to December 2014 (MODIS) and January 2012 to December 2016 (VIIRS), respectively (Fig. 1). The NASA standard atmospheric

correction algorithm with the near-infrared (NIR) radiance corrections (Bailey et al., 2010; Stumpf et al., 2003) is used to derive both the MODIS-Aqua and the VIIRS level-2 ocean color data. The MODIS and VIIRS Chl-a data are obtained using the NASA standard ocean color chlorophyll algorithm for MODIS (OC3M; O'Reilly et al., 2000). The daytime SST products from the MODIS and VIIRS data are derived using the long-wave SST algorithm with MODIS bands at 11 and 12 μm (Minnett et al., 2004). More information about the MODIS-Aqua and VIIRS Level-2 data can be found at the NASA ocean color website. The Level-2 data were remapped at 1 × 1 km spatial resolution for the Korean mid-west coasts (KMWC) with a standard Mercator projection.

The MODIS and VIIRS total suspended sediments (TSS) data were generated using the regional TSS model (Siswanto et al., 2011; Son et al., 2014) to create TSS maps in KMWC as follows:

$$Log(TSS) = 0.649 + 25.623 \cdot [R_{rs}(555) + R_{rs}(670)] - 0.646 \cdot \frac{R_{rs}(490)}{R_{rs}(555)} \quad (1)$$

The satellite climatology composite images of Chl-a, SST, and TSS in 2002–2016 were derived from the daily MODIS- and VIIRS-derived products to characterize the temporal and spatial variation of Chl-a, SST, and TSS in the study area (Fig. 2). Data collected from pixels in region A, B, and C were spatially averaged for each sampling month, which were then used for multiple regression analyses (model development).

2.4. Data analysis

To identify the most correlated environmental factors for DO variation, the linear relationship with a correlation coefficient was analyzed. The *in situ* water quality data within each region A, B, and C were spatially averaged to get a single value for the corresponding months. A total of 166 samples were available during the 2002–2016 period, excluding data points of null values. The seasonal time series of each environmental variable was correlated with the DO data. A total of fifteen variables were compared in coastal waters: water temperature, SS, Chl-a, salinity, pH, COD, ammonia, nitrite, nitrate, DIN, TN, DIP, TP, silicate, and Secchi depth.

In order to develop an empirical algorithm to estimate DO from satellite data, *in situ* observed DO and satellite-derived data were used in the stepwise multiple regression analysis. Monthly satellite-derived SST, Chl-a, and TSS data were also averaged for each box (A–C in Fig. 1) producing a total of 166 vectors. For those satellite data, the monthly average values in the sampling month (SST, Chl-a, and TSS) as well as the monthly average values one month prior to the sampling (SST_{m-1}, $Chl\text{-}a_{m-1}$, and TSS_{m-1}) were used as input variables to incorporate potential delayed effects (e.g., Kim et al., 2017; Yang et al., 2018). Of the 166 data samples, one half (83 samples) were randomly selected for the stepwise multiple regression and the other half (83 samples) were used for validating the algorithm. Both sets of the model development and validation samples represent well the statistical characteristics of the population, and they show wide levels of DO concentrations and no bias in seasonality. In each step of stepwise multiple regression, a predictive (input) variable is added to the model when it has an F-value that is greater than two. Normality of residuals is tested using Kolmogorov-Smirnov and Shapiro-Wilk's W. Autocorrelation of residuals is checked by Durbin-Watson statistic. The residual statistics are given in supplementary Table S2. To evaluate the algorithm performance, two error parameters including the absolute relative error (ARE) and index of agreement (IOA) were calculated (Wilmott et al., 2012). Both of the correlation and multiple regression analyses were examined using SPSS 12.0.

3. Results and discussion

3.1. Long-term environmental condition based on the in-situ monitoring system

The data collected from the K-MEMS, including temperature, salinity, SS, Chl-a, pH, DO, COD, ammonia, nitrite, nitrate, DIN, TN, DIP, TP, silicate, and Secchi depth, show the environmental variability for the period between 2002 and 2016. In order to evaluate the long-term variability pattern, the data from each station were spatially averaged for each region. Fig. 3 shows all available data for three regions outside of the Saemangeum dike during the study period of 2002–2016.

The temperature in all three regions was relatively uniform and is characterized by a distinct pattern of seasonal variability ranging from 2 °C during winter to 28 °C during summer (Fig. 3a). Such spatial homogeneity can also be found in several other water quality parameters like Chl-a, pH, DO, and DIP, TP. In contrast, spatial variability in salinity shows clearly that the regions B and C (e.g., offshore of the Saemangeum dike) have water masses different than that of the region A that is under the influence of substantial input of freshwater from Geum River. Salinity in the region A was higher ranging from 15 and

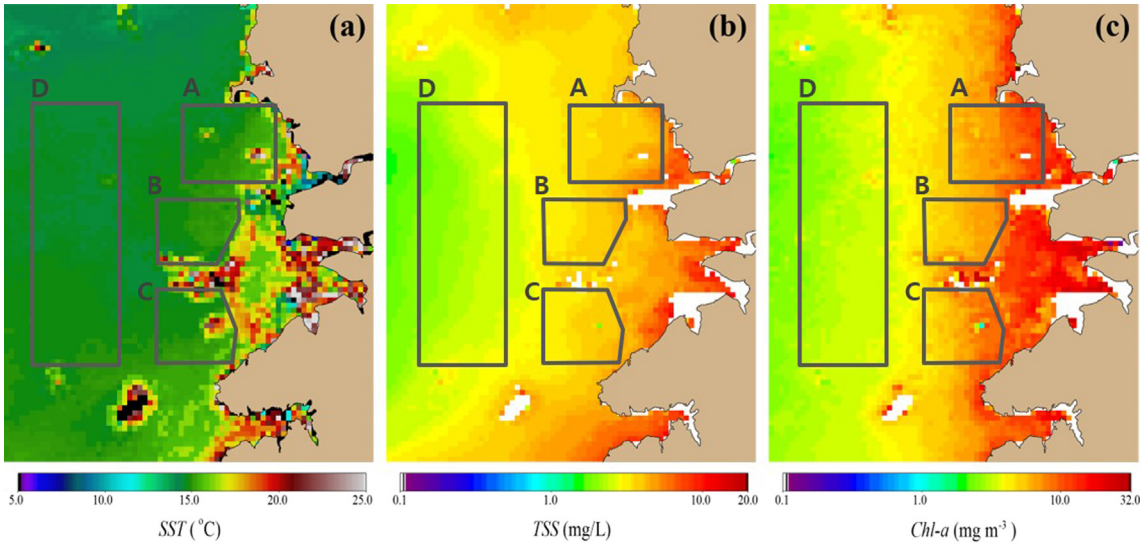

Fig. 2. Climatology of (a) satellite-derived sea surface temperature (SST), (b) total suspended solids (TSS), and (c) chlorophyll-a based on the MODIS and VIIRS satellite data collected during 2002–2016. Data for model development were monthly averaged within boxes (dark grey). (For interpretation of the references to colour in this figure legend, the reader is referred to the web version of this article.)

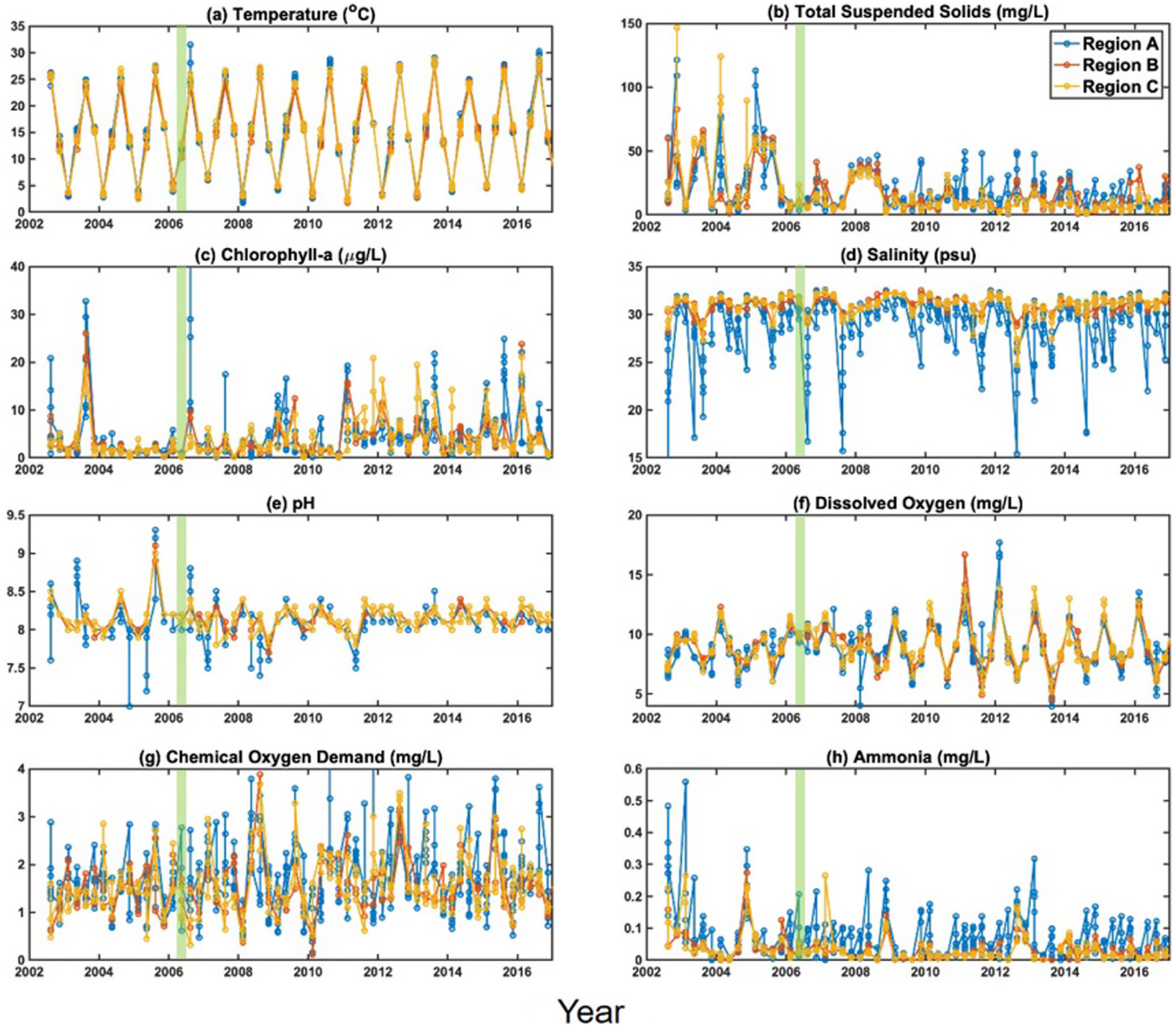

Fig. 3. Long-term seasonal variations of surface *in situ* water quality parameters during 2002–2016. Dike construction was completed in April 2006 (light green bar): (a) water temperature, (b) total suspended solids, (c) chlorophyll-a, (d) salinity, (e) pH, (f) dissolved oxygen, (g) chemical oxygen demand, (h) ammonia, (i) nitrite, (j) nitrate, (k) dissolved inorganic nitrogen, (l) total nitrogen, (m) dissolved inorganic phosphorus, (n) total phosphorus, (o) silicate, and (p) Secchi depth. Blue, red, and yellow lines represent the data from region A, B, and C in Fig. 1, respectively. (For interpretation of the references to colour in this figure legend, the reader is referred to the web version of this article.)

33, while that in the regions B and C did not go below 25 (Fig. 3d and Table S1). Such spatial variation was also found in several other water quality parameters, including ammonia, nitrite, nitrate, DIN, TN, and silicate (Fig. 3 and Table S1), which are mostly considered as river-driven materials.

Temporal variability of SS in regions B and C (i.e., offshore of the dike) were relatively higher during years before 2006, while it shows lower SS concentration after 2006 (Fig. 3b and Table S1). This change must be related to the completion of the dike construction project at 2006, after which less input of suspended materials from the land occurred (Son and Wang, 2009).

A similar change in the temporal pattern before and after 2006 is also observed in ammonia, nitrate, DIN, TN, DIP and TP (Fig. 3 and Table S1). The change before and after 2006 can be summarized as an significant increase in COD ($p < 0.05$), an increase in the range of DO, and a significant decrease in the average level of SS, ammonia, nitrate, DIN, TN, DIP and TP (Table S1). Unraveling reasons for the changes in those environmental parameters is beyond the scope of this paper, but we can speculate that they must be related to the dike construction.

3.2. Correlation analysis of DO with environmental monitoring variables

Pearson correlation analysis was performed between DO at the surface layer and various water quality data collected from the K-MEMS database (Table 1). The variables with significant correlation ($p < 0.05$) include temperature, salinity, Chl-a, COD, ammonia, nitrite, nitrate, DIN, TN, DIP, TP, silicate, and turbidity (i.e., Secchi depth). The correlation coefficients for some variables, such as temperature with DO, are larger than 0.7 (ranging -0.743 to -0.792), indicating that temperature and DO are inversely related.

Such an inverse relationship is also noticeable in the scatter plot and time-series comparison between temperature and DO in surface waters (Fig. 4). During the summer months when the temperature is high, DO is low, and vice versa. Based on the formula proposed by Benson and Krause (1980, 1984) and Weiss (1970), percent saturation of DO was 86.7 ± 12.0% in region A with the range of 29.5–140.4%. Region B

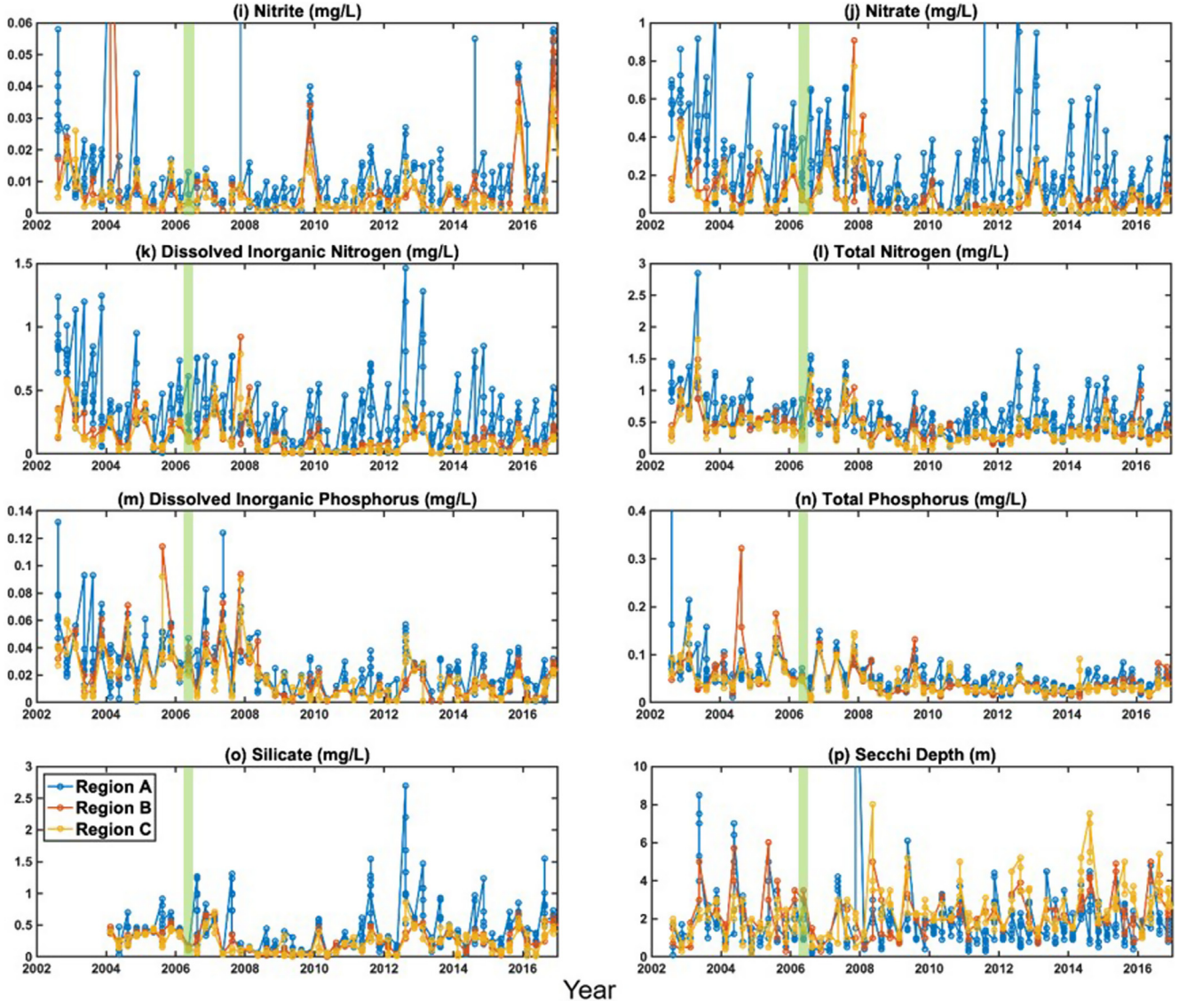

Fig. 3. (*continued*)

Table 1
Pearson correlation coefficient and *p*-value by correlation analysis between *in situ* DO and other *in situ* water quality parameters in four regions of Saemangeum area.

Parameters	Region A (n = 464)		Region B (n = 464)		Region C (n = 464)		Region D (n = 464)	
	Coefficient	*p*	Coefficient	*p*	Coefficient	*p*	Coefficient	*p*
Temp.	−0.743	< 0.001	−0.792	< 0.001	−0.785	< 0.001	−0.646	< 0.001
SS	−0.024	0.599	−0.032	0.723	0.039	0.599	0.124	< 0.01
Chl-a	0.067	0.147	0.307	< 0.001	0.314	< 0.001	0.085	< 0.05
Salinity	0.315	< 0.001	0.342	< 0.001	0.405	< 0.001	0.255	< 0.001
pH	−0.015	0.751	−0.077	0.387	−0.055	0.459	0.066	0.109
COD	−0.11	< 0.05	−0.086	0.336	−0.118	0.108	−0.066	0.113
Ammonia	−0.135	< 0.01	−0.185	< 0.05	−0.16	< 0.05		
Nitrite	−0.147	< 0.01	0.007	0.938	−0.107	0.145		
Nitrate	−0.043	0.356	0.179	< 0.05	0.2	0.006		
DIN	−0.054	0.244	0.111	0.213	0.098	0.182		
TN	−0.101	< 0.05	0.139	0.118	0.131	0.074	−0.089	< 0.05
DIP	−0.143	< 0.01	−0.09	0.313	−0.162	< 0.05		
TP	−0.133	< 0.01	−0.122	0.171	−0.142	0.053	−0.307	< 0.001
Silicate	−0.2	< 0.001	−0.093	0.322	−0.115	0.137		
Secchi d.	−0.062	0.182	−0.216	< 0.05	−0.368	< 0.001		

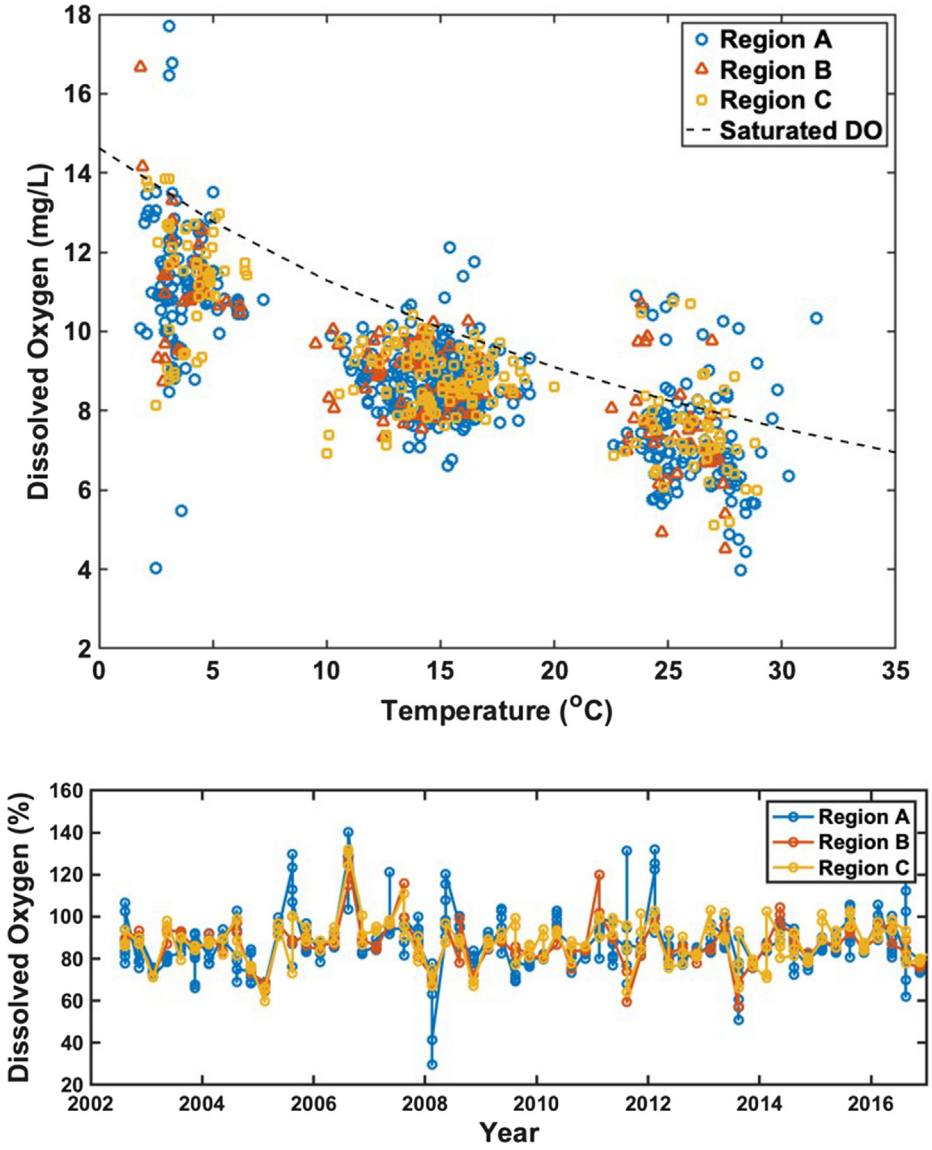

Fig. 4. Scatter plot of temperature and DO presented as mg/L (upper), and time-series of DO converted into the percent saturation (lower) in surface waters of the study area based on *in situ* observation data.

showed 86.9 ± 10.5% and ranged between 57.3% and 126.5%. Region C averaged 88.3 ± 10.8% from the minimum of 59.6% to the maximum of 131.8% of DO saturation. In most cases, near-saturated DO conditions were indicated (Fig. 4). Of note, region A showed two cases of lower DO in February of 2008 at 4.03 mg/L, an equivalent of 29.5% DO at 2.5 °C, and 5.48 mg/L, 41.4% DO at 3.5 °C. The development and growth of salmonid fish embryos could be affected by any reduced DO from the air-saturation level or from a higher level, even at favorable temperatures (Doudoroff and Shumway, 1970). Therefore, it is important to monitor DO level in coastal and estuarine areas in near air-saturated conditions with high spatial and temporal resolutions.

3.3. Multiple regression analysis of DO with satellite-derived variables

Six satellite-derived parameters of SST, TSS, and Chl-a during the present and previous month were used to estimate *in situ* DO by applying a multiple regression analysis. By the stepwise multiple regression, a model with the highest determination coefficient was selected (Table S2). The results show a strong correlation ($R^2 = 0.801$, $p < 0.001$) of DO observed *in situ* with a linear combination of SST (°C), SST_{m-1} (SST in one month prior, °C) and Chl-a_{m-1} (Chl-a in one month prior, μg/L) (Table 2). Multicollinearity of three independent variables were checked using variance inflation factor, and SST and SST_{m-1} showed relatively high collinearity among independent variables (SST: 2.560, SST_{m-1}: 2.362, Chl-a_{m-1}: 1.175). In spite of potential multicollinearity issue, those three variables were selected for input variables based on the results of stepwise multiple regression results (Table S2). Residuals were normally distributed as the Kolmogorov-Smirnov ($p = 0.2$) and Shapiro-Wilk statistic ($p = 0.16$) indicated. Results of residual analysis verifies the applicability of regression model selected. The existence of influential and outlier observations was not found in the model (Table S3). Based on the results of the multiple regression analysis, an empirical DO algorithm can be derived as:

$$DO = -0.131 \cdot SST - 0.132 \cdot SST_{m-1} + 0.066 \cdot Chl - a_{m-1} + 12.343 \quad (2)$$

The satellite-derived DO data that are monthly- and spatially-averaged for each box in Fig. 1 were compared with the *in situ* DO to evaluate the performance of the developed algorithm. Two error indices, ARE and IOA, were calculated for the other half of data samples that were not used for the algorithm development (Table 2). The error estimate results show high values of 89.2% for 1-ARE and 78.6% of IOA, indicating the reliable performance of our model to retrieve the

Table 2
Result of multiple regression analysis between *in situ* dissolved oxygen (DO) of surface waters and satellite parameters.

Coefficient			Constant	R^{2**}	*p*	Validation	
SST	Chl-a_{m-1}*	SST_{m-1}*				1-ARE	IOA
−0.131	0.066	−0.132	12.343	0.801	< 0.001	89.2%	78.6%
−0.507[a]	−0.480[a]	0.042[a]					

* satellite data of one month prior to *in situ* measuring.
** modified coefficient of determination considering the degree of freedom.
[a] standardized coefficient (unitless).

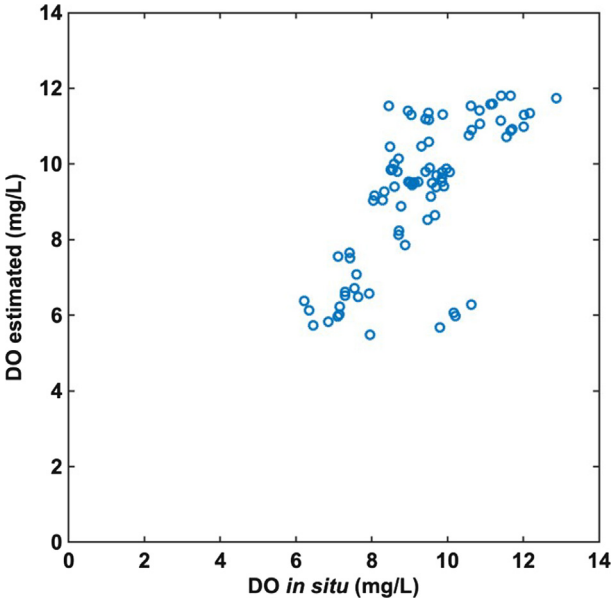

Fig. 5. Scatter plot of DO *in situ* and DO estimated from the satellite-based model.

DO from the satellite data (Fig. 5). Some outliers can be found on the right bottom corner of Fig. 5, which represents underestimation of DO by the model developed in this study. Those particular samples were observed in August of 2006 and 2007 when the water temperature exceeded over 27 °C and *in situ* DO was over-saturated more than 120%. It may imply that one should be careful when applying this DO model under the circumstance of relatively high water temperature.

The Eq. (2) was applied to all monthly composite MODIS and VIIRS data collected during 2002 and 2016 period. Monthly DO values were retrieved by using the empirical algorithm, presenting a monthly DO map for the study area (Fig. 6). The satellite-derived DO shows high-resolution spatial variability offshore of Saemangeum dike, with the exception of some null data points near the coastline and inside the Saemangeum dike (shown as blank white pixels in Fig. 6).

3.4. Temporal and spatial variability of DO offshore Saemangeum dike

The DO concentration is one of the most commonly used water quality indicators in coastal and ocean environments (Breitburg et al., 2018; Diaz and Rosenberg, 2008). In particular, water quality index (WQI) used by Korean government agencies is heavily dependent on the bottom DO concentration in the water column (Ministry of Oceans and Fisheries, 2013b), which has been used for evaluation of coastal management practices in Korea. That is why, as part of K-MEMS, the DO at the surface and bottom water has been measured in the vicinity of Saemangeum dike during the past decades. Based on these *in situ* observation datasets, Fig. 7 shows the temporal change of DO offshore Saemangeum (region D in Fig. 1). The results show a clear seasonal cycle, whereby relatively high DO during winter (February) and lowest DO during summer (August). Since the *in situ* measured data were only collected every three months, it may only be able to show the seasonal variability. The datasets cannot prove whether higher-frequency variabilities like monthly patterns exist, due to the limited data frequency.

In order to evaluate monthly variability of DO concentration, monthly-composite satellite data were used to generate the distribution of DO concentration offshore Saemangeum area. Fig. 6a and b show the spatial variability of the DO during August and September 2003, respectively, depicting the water quality condition before the completion of dikes. One can see that there is relatively higher surface DO distribution during August than September in 2003 (i.e., relativerly brighter blue in 6a than 6b). Additionally, this change is more noticeable in the northern region than in the southern region. It implies that the satellite-derived approach can provide more synoptic and consistent DO concentration in the study area.

Fig. 6c and d show the DO during August and September 2012, respectively, representing the water quality conditions after the completion of the dike construction. When compared to the condition of 2003, it shows much lower satellite-derived DO during 2012. Such lower DO during summer as well as higher DO in winter after the completion of dike construction are also confirmed in the *in situ* observation data (see Figs. 3f and 4).

In order to show applicability of the DO model developed in this study, several satellite-based environmental parameters including DO concentration are derived for offshore Saemangeum and spatially-averaged for region D (see Fig. 1 for the location) in each month for the past 15 years during 2002–2016. There is no monitoring system available for region D, so the satellite-derived environmental variables would be considered best available data sets for any environmental management practice. The change in environmental conditions between before and after the dike construction can also be observed in Fig. 7, with better temporal resolution, i.e., monthly variability. The noticeable change in Chl-a is seen before and after 2006, along with the change in SST, TSS, and DO, although the latter ones are not as prominent as Chl-a.

The study area, where the spatial averaging was calculated, is located directly offshore of the Saemangeum dike, one of the largest sea dikes of 33.9 km long. After the completion of the dikes in April 2006, the coastal area experienced significant environmental changes such as modified tidal currents (Choi et al., 2010; Lee and Lee, 2012; Park et al., 2014), waves (Lee and Ryu, 2008; Lee, 2010), and sediment transport patterns (Lee et al., 2008; Min et al., 2012). The limited river discharge also occurred (Son and Wang, 2009), which results in strong influences on the benthic ecosystem (Ryu et al., 2014). The construction of dikes across the two river mouths (Dongjin and Mangyeong Rivers) has also resulted in reduced input of freshwater and of land-borne materials, such as nutrients, which was also observed at the satellite remote sensing scale (Son and Wang, 2009). This change in hydrographic and environmental settings may induce the long-term variability in environmental variables including DO concentration, shown in Figs. 3f and 4. It should be noted, however, that such change is not clearly observed in the satellite-derived environmental conditions in region D (Fig. 7) since that area might be relatively distant from the direct influence of the dike construction. More details about the causes and

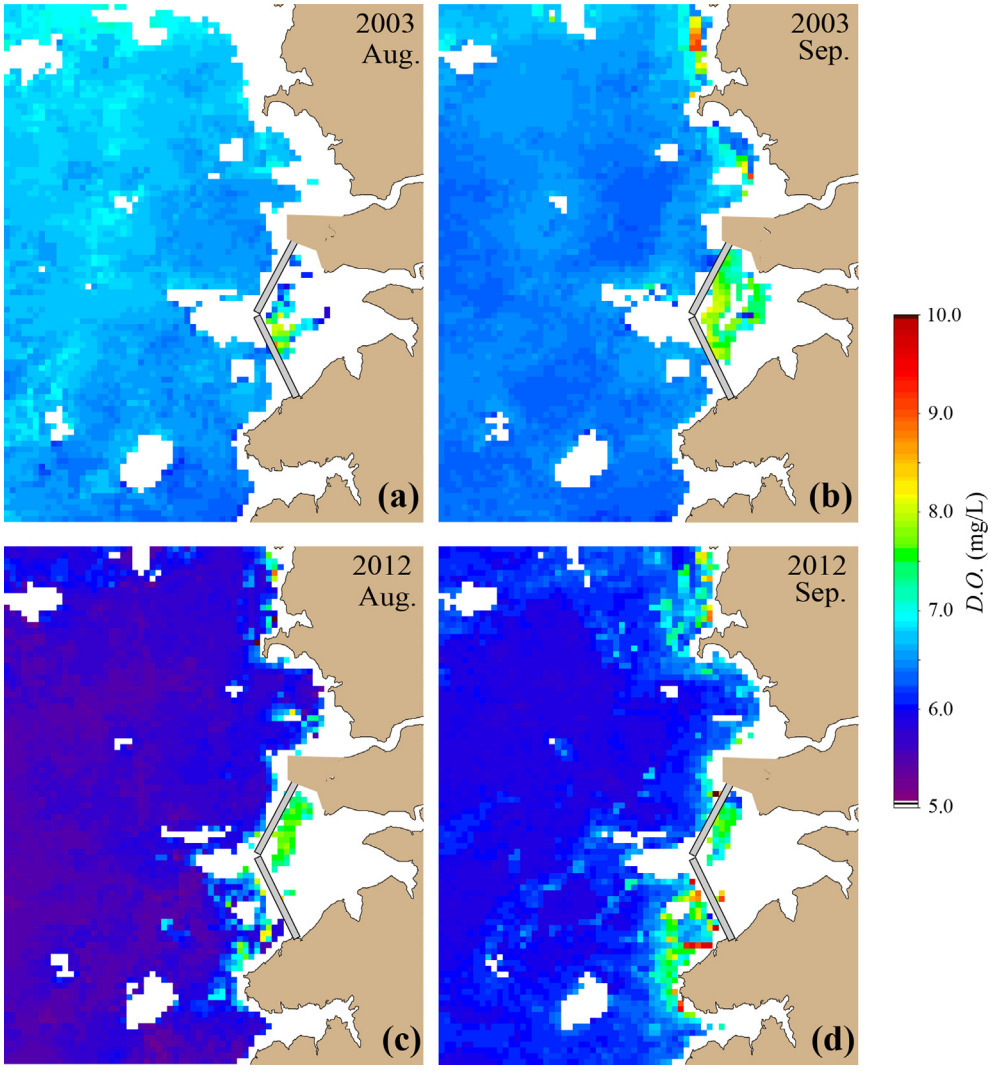

Fig. 6. Spatial distribution of the dissolved oxygen (DO) concentration derived from MODIS data offshore Saemangeum dike during Aug 2003 (a), Sep 2003 (b), Aug 2012 (c), and Sep 2012 (d). Blank white pixels represent no data available for those locations.

impacts of environmental changes induced by the dike construction, e.g., why and how the DO regime changed or what extent of such environmental impacts were, are beyond the scope of this study.

4. Novelty and limitations

Recently, science-based environmental management decision and planning approaches have been widely applied to various environments including coastal environments. One of obstacles can be having difficult to find appropriate scientific data sets for target areas in broad as well as detail coverages of both temporal and spatial perspective. The present study can provide potential solutions for such problems with the findings that the satellite-derived environmental variables, including SST, TSS, Chl-a, and DO, would be used as valuable scientific foundations to understand the long-term environmental changes with both higher temporal and spatial resolution. One of examples may be shown in Fig. 7, which depicts the temporal variability of such environmental variables in the region D where there is no monitoring data available. Thus, further analysis of various satellite-derived environmental parameters will provide a strong foundation of understanding in environmental changes. This could be critical in building improved prediction models that will act as decision-supporting tools and enable to simulate environmental and ecosystem changes. Thus, proper management decision and planning can be established on the basis of these scientific findings. At this juncture, it should be noted that such RS data could also have the following limitations: (1) that the RS data can provide environmental conditions of surface waters, so users should be careful to apply such approaches in area where strong vertical variability exists; and (2) that the RS data are indirect measurements of environmental varialbes so they need to be ground-truthed to increase confidence levels.

5. Conclusions

High resolution of DO data in surface waters can be retrieved from satellite-derived SST and Chl-a by multiple regression analysis. Principally, DO and water temperature show a strong inverse relationship, which is consistent with the gas solubility law. In this study, a multiple regression model was developed to estimate DO in surface waters based on the comparison of *in situ* DO observation data with satellite-derived water temperature and Chl-a concentration. Using the satellite-derived DO algorithm, long-term changes in DO concentration can be detected, which can provide the difference in DO before and after the dike construction in Saemangeum, Korea. In the coastal area of Korea, over 400 stations used to monitor water quality in coastal areas seasonally have been operated since 1997; data have been used for the evaluation of coastal management practices in order to enhance water quality. With the help of the approach proposed in this study, the water

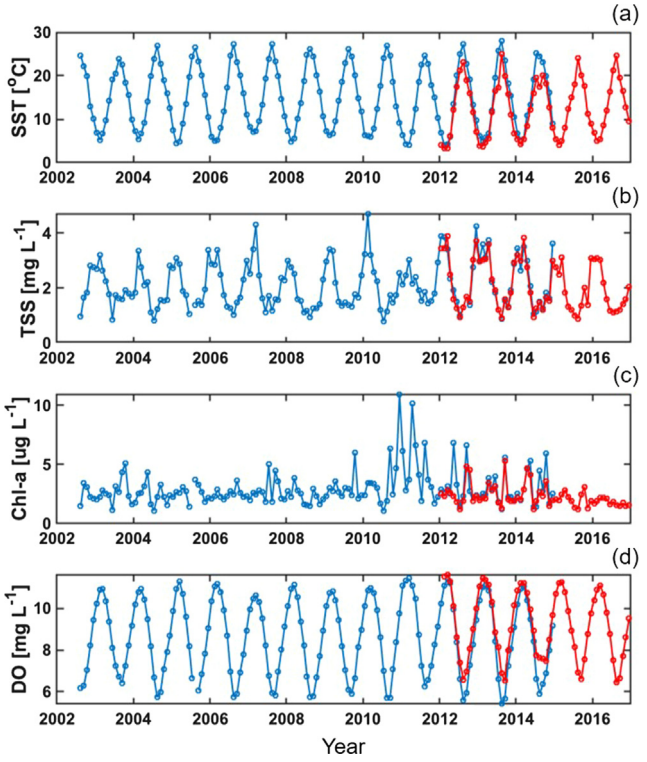

Fig. 7. Long-term variability of (a) sea surface temperature (SST), (b) total suspended solids (TSS), (c) chlorophyll-a (Chl-a) concentration, and (d) dissolved oxygen (DO) concentration derived from satellite data offshore Saemangeum (region D in Fig. 1). Blue lines represent MODIS-derived data (2002–2014), and red lines represent VIIRS-derived data (2012–2016). (For interpretation of the references to colour in this figure legend, the reader is referred to the web version of this article.)

quality measures, including DO concentration, will be extended to a higher resolution both in space and time. The outlined approach demonstrates the potential applicability of satellite remote sensing data to understand environmental changes in coastal areas, useful for appropriate management planning and future implementation.

Declaration of Competing Interest

The authors declared that there is no conflict of interest.

Acknowledgments

The Ministry of Oceans and Fisheries (Republic of Korea) supported this work (Grant No. 20140257; 20140431; 20170325).

Appendix A. Supplementary material

Supplementary data to this article can be found online at https://doi.org/10.1016/j.envint.2019.105301.

References

Bailey, S.W., Franz, B.A., Werdell, P.J., 2010. Estimation of near-infrared water-leaving reflectance for satellite ocean color data processing. Opt. Express 18, 7521–7527.
Benson, B.B., Krause, D., 1980. The concentration and isotopic fractionation of gases dissolved in freshwater in equilibrium with the atmosphere 1. Oxtgen. Limnol. Oceanogr. 25, 662–671.
Benson, B.B., Krause, D., 1984. The concentration and isotopic fractionation of oxygen dissolved in freshwater and seawater in equilibrium with the atmosphere. Limnol. Oceanogr. 29, 620–632.
Breitburg, D., Levin, L.L., Oschlies, A., Gregoire, M., Chavez, F.P., Conley, D.J., Garcon, V., Gilbert, D., Gutierrez, D., Isensee, K., Jacinto, G.S., Limburg, K.E., Montes, I., Naqvi, S.W.A., Pitcher, G.C., Rabalais, N.N., Roman, M.R., Rose, K.A., Seibel, B.A., Telszewski, M., Yasuhara, M., Zhang, J., 2018. Declining oxygen in the global ocean and coastal waters. Sci. 359 eaam7240.
Choi, B.H., Kim, K.O., Lee, H.S., Yuk, J.H., 2010. Perturbation of regional ocean tides due to coastal dikes. Cont. Shelf Res. 30, 553–563.
Choi, J.K., Park, Y.J., Ahn, J.H., Lim, H.S., Eom, J., Ryu, J.H., 2012. GOCI, the world's first geostationary ocean color observation satellite, for the monitoring of temporal variability in coastal water turbidity. J. Geophys. Res. 117, C09004.
Choi, K., Kim, S.-P., 2006. Later quaternary evolution of macrotidal Kimpo tidal flat, Kyonggi Bay, west coast of Korea. Mar. Geol. 232, 17–34.
Diaz, R.J., Rosenberg, R., 2008. Spreading dead zones and consequences for marine ecosystems. Sci. 321, 926–929.
Doudoroff, P., Shumway, D.L., 1970. Dissolved oxygen requirements of freshwater fishies. FAO Fish. Tech. Pap. No. 86, Food and Agriculture Organization of the United Nations, Rome.
Farrell, A.P., 2016. Pragmatic perspective on aerobic scope: peaking, plummeting, pejus and apportioning. J. Fish Biol. 88, 322–343.
Gholizadeh, M.H., Melesse, A.M., Reddi, L., 2016. A comprehensive review on water quality parameters estimation using remote sensing techniques. Sensors 16, 1298.
Gobler, C.J., Baumann, H., 2016. Hypoxia and acidification in ocean ecosystems: coupled dynamics and effects on marine life. Biol. Lett. 12, 20150976.
Goetz, S., Gardiner, N., Viers, J., 2008. Monitoring freshwater, estuarine and near-shore benthic ecosystems with multi-sensor remote sensing: an introduction to the special issue. Remote Sens. Environ. 112, 3993–3995.
Harvey, E.T., Kratzer, S., Philipson, P., 2015. Satellite-based water quality monitoring for improved spatial and temporal retrieval of chlorophyll-a in coastal waters. Remote Sens. Environ. 158, 417–430.
Hellweger, F.L., Schlosser, P., Lall, U., Weissel, J.K., 2004. Use of satellite imagery for water quality studies in New York Harbor. Estuar. Coast. Shelf Sci. 61, 437–448.
Hwang, J.H., Van, S.P., Choi, B.-J., Chang, Y.S., Kim, Y.H., 2014. The physical processes in the Yellow Sea. Ocean Coast. Manage. 102, 449–457.
Keeling, R.F., Krtzinger, A., Gruber, N., 2010. Ocean deoxygenation in a warming world. Ann. Rev. Mar. Sci. 2, 463–493.
Kilpatrick, K.A., Podesta, G., Walsh, S., Williams, E., Halliwell, V., Szczodrak, M., Brown, O.B., Minnett, P.J., Evans, R., 2015. A decade of sea surface temperature from MODIS. Remote Sens. Environ. 165, 27–41.
Kim, H.-C., Son, S., Kim, Y.H., Khim, J.S., Nam, J., Chang, W.K., Lee, J.-H., Lee, C.-H., Ryu, J., 2017. Remote sensing and water quality indicators in the Korean West coast: Spatio-temporal structures of MODIS-derived chlorophyll-a and total suspended solids. Mar. Pollut. Bull. 121, 425–434.
Kim, Y.H., Im, J., Ha, H.K., Choi, J.-K., Ha, S., 2014. Machine learning approaches to coastal water quality monitoring using GOCI satellite data. Gisci. Remote Sen. 51, 158–174.
Lee, H.J., 2010. Enhanced movements of sands off the Saemangeum Dyke by an interplay of dyke construction and winter monsoon. Coastal Environmental and Ecosystem Issues of the East China Sea. In: Ishimatsu, A., Lie, H.J. (Eds.), Coastal Environmental and Ecosystem Issues of the East China Sea. TERRAPUB, Tokyo, pp. 49–70.
Lee, H.J., Lee, S.H., 2012. Geological consequences of the Saemangeum Dyke, mid-west coast of Korea: a review. Ocean Sci. J. 47, 395–410.
Lee, H.J., Ryu, S.O., 2008. Changes in topography and surface sediments by the Saemangeum dyke in an estuarine complex, west coast of Korea. Cont. Shelf Res. 28, 1177–1189.
Lee, S., Lie, H., Song, K., Cho, C., Lim, E., 2008. Tidal modification and its effect on sluice-gate outflow after completion of the Saemangeum dike, South Korea. J. Oceanogr. 64, 763–776.
Middelburg, J., Levin, L.A., 2009. Coastal hypoxia and sediment biogeochemistry. Biogeosci. 6, 1273–1293.
Miller, R., McKee, B., 2004. Using MODIS terra 250 m imagery to map concentrations of total suspended matter in coastal waters. Remote Sens. Environ. 93, 259–266.
Min, J.-E., Ryu, J.-H., Lee, S., Son, S., 2012. Monitoring of suspended sediment variation using Landsat and MODIS in the Saemangeum coastal area of Korea. Mar. Pollut. Bull. 64, 382–390.
Ministry of Oceans and Fisheries, 2013a. Water quality experiment manual according to Article 10 of Marine Environment Management Act.
Ministry of Oceans and Fisheries, 2013b. Water quality index in marine environments according to Article 8 of Marine Environment Management Act. http://www.meis.go.kr/rest/wqi_calculate.
Minnett, P.J., Brown, O.B., Evans, R.H., Key, E.L., Kearns, E.J., Kilpatrick, K., Kumar, A., Maillet, K.A., Szczodrak, G., 2004. Sea-surface temperature measurements from the Moderate-Resolution Imaging Spectroradiometer (MODIS) on Aqua and Terra. Geoscience and Remote Sensing Symposium, 2004. IGARSS'04. Proceedings. 2004 IEEE International. IEEE, pp. 4576-4579.
O'Reilly, J.E., Maritorena, S., O'Brien, M., Siegel, D., Toole, D., Menzies, D., Smith, R., Mueller, J., Mitchell, B.G., Kahru, M., 2000. SeaWiFS postlaunch calibration and validation analyses, part 3. NASA Tech. Memo 206892, 3–8.
Park, Y.-G., Kim, H.-Y., Hwang, J.H., Kim, T., Park, S., Nam, J.-H., Seo, Y.-K., 2014. Dynamics of dike effects on tidal circulation around Saemangeum. Korea. Ocean Coast. Manage. 102, 572–582.
Rabalais, N.N., 2004. Eutrophication. In: Robinson, A.R., Brink, K. (Eds.), The Sea, Volume 13: The Global Coastal Ocean: Multiscale Interdisciplinary Processes. Harvard University Press, Cambridge, pp. 819–865.
Rabalais, N.N., Harper Jr., D.E., Turner, R.E., 2001. Responses of nekton and demersal and benthic fauna to decreasing oxygen concentrations. In: Rabalais, N.N., Turner, R.E. (Eds.), Coastal Hypoxia: Consequences for Living Resources and Ecosystems. Coastal and Estuarine Stud. 58. American Geophysical Union, Washington DC, pp. 115–128.
Ryu, J., Khim, J.S., Choi, J.-W., Shin, H.C., An, S., Park, J., Kang, D., Lee, C.-H., Koh, C.-

H., 2011. Environmentally associated spatial changes of a macrozoobenthic community in the Saemangeum tidal flat. Korea. J. Sea Res. 65, 390–400.
Ryu, J., Nam, J., Park, J., Kwon, B.-O., Lee, J.-H., Song, S.J., Hong, S., Chang, W.K., Khim, J.S., 2014. The Saemangeum tidal flat: Long-term environmental and ecological changes in marine benthic flora and fauna in relation to the embankment. Ocean Coast. Manage. 102, 559–571.
Sharaf El Din, E., Zhang, Y., Suliman, A., 2017. Mapping concentrations of surface water quality parameters using a novel remote sensing and artificial intelligence framework. Int. J. Remote Sens. 38, 1023–1042.
Shen, L., Xu, H., Guo, X., 2012. Satellite remote sensing of harmful algal blooms (HABs) and a potential synthesized framework. Sensors 12, 7778–7803.
Siswanto, E., Tang, J., Yamaguchi, H., Ahn, Y.-H., Ishizaka, J., Yoo, S., Kim, S.-W., Kiyomoto, Y., Yamada, K., Chiang, C., 2011. Empirical ocean-color algorithms to retrieve chlorophyll-a, total suspended matter, and colored dissolved organic matter absorption coefficient in the Yellow and East China Seas. J. Oceanogr. 67, 627–650.
Son, S., Wang, M., 2009. Environmental responses to a land reclamation project in South Korea. Eos 90, 398–399.
Son, S., Wang, M., 2012. Water properties in chesapeake bay from modis-aqua measurements. Remote Sens. Environ. 123, 163–174.
Son, S., Kim, Y.H., Kwon, J.-I., Kim, H.-C., Park, K.-S., 2014. Characterization of spatial and temporal variation of suspended sediments in the yellow and East China Seas using satellite ocean color data. Gisci. Remote Sens. 51, 212–226.
Stumpf, R.P., Arnone, R., Gould, R., Martinolich, P., Ransibrahmanakul, V., 2003. A partially coupled ocean-atmosphere model for retrieval of water-leaving radiance from SeaWiFS in coastal waters. NASA Tech. Memo 206892, 51–59.
Weiss, R.F., 1970. The solubility of nitrogen, oxygen and argon in water and seawater. Deep Sea Res. Oceanogr. Abstr. 17, 721–735.
Wilmott, C.J., Robeson, S.M., Matsuura, K., 2012. A refined index of model performance. Int. J. Climatol. 32, 2088–2094.
Yang, Y., Chui, T.F.M., Shen, P.P., Yang, Y., Gu, J.D., 2018. Modeling the temporal dynamics of intertidal benthic infauna biomass with environmental factors: Impact assessment of land reclamation. Sci. of Total Env. 618, 439–450.
Zhang, M., Tang, J., Dong, Q., Song, Q., Ding, J., 2010. Retrieval of total suspended matter concentration in the Yellow and East China Seas from MODIS imagery. Remote Sens. Environ. 114, 392–403.